BACK PAIN

# Parathyroid hormone treatment partially reverses endplate remodeling and attenuates low back pain in animal models of spine degeneration

Zemin Ling[1,2]†, Janet Crane[1,3]†, Hao Hu[2]†, Yan Chen[2], Mei Wan[1], Shuangfei Ni[1], Shadpour Demehri[4], Bahram Mohajer[4], Xinsheng Peng[2], Xuenong Zou[2]*, Xu Cao[1]*



**Low back pain (LBP) is one of the most prevalent diseases affecting quality of life, with no disease-modifying therapy. During aging and spinal degeneration, the balance between the normal endplate (EP) bilayers of cartilage and bone shifts to more bone. The aged/degenerated bony EP has increased porosity because of osteoclastic remodeling activity and may be a source of LBP due to aberrant sensory innervation within the pores. We used two mouse models of spinal degeneration to show that parathyroid hormone (PTH) treatment induced osteogenesis and angiogenesis and reduced the porosity of bony EPs. PTH increased the cartilaginous volume and improved the mechanical properties of EPs, which was accompanied by a reduction of the inflammatory factors cyclooxygenase-2 and prostaglandin $E_2$. PTH treatment furthermore partially reversed the innervation of porous EPs and reversed LBP-related behaviors. Conditional knockout of PTH 1 receptors in the nucleus pulposus (NP) did not abolish the treatment effects of PTH, suggesting that the NP is not the primary source of LBP in our mouse models. Last, we showed that aged rhesus macaques with spontaneous spinal degeneration also had decreased EP porosity and sensory innervation when treated with PTH, demonstrating a similar mechanism of PTH action on EP sclerosis between mice and macaques. In summary, our results suggest that PTH treatment could partially reverse EP restructuring during spinal regeneration and support further investigation into this potentially disease-modifying treatment strategy for LBP.**

## INTRODUCTION

Spinal degeneration with low back pain (LBP) is one of the most prevalent diseases causing frailty and a decline in mobility (*1*, *2*). LBP is the leading cause of work absence throughout much of the world and a major reason to seek medical treatment (*3*). Unfortunately, 90% of LBP is nonspecific, and the cause of LBP is often unknown because no abnormality other than degeneration of intervertebral discs (IVDs) is observed (*4*, *5*). Four commonly used classes of medications for LBP are paracetamol, opioids, nonsteroidal anti-inflammatory drugs [NSAIDs; including cyclooxygenase-2 (COX-2) inhibitors], and skeletal muscle relaxants (*6*). When the traditional medications are properly administrated according to the World Health Organization analgesic ladder, LBP can be effectively relieved; however, their side effects range from addiction, respiratory depression, and constipation (opioids); hepatorenal toxicity (paracetamol); or gastrointestinal and cardiovascular damage (NSAIDs). LBP is prone to recurrence after drug withdrawal. Currently, no disease-modifying therapy is available for LBP.

Pathological changes in the various spinal components are associated with pain and accelerated aging (*7*). Recent studies showed involvement of the vertebral endplate (EP) in the development of spinal degeneration and LBP (*8*–*10*). The EP is a complex structure composed of a bony layer and a cartilage layer and forms a structural boundary between the IVD and vertebral body. EPs transmit mechanical loads from body weight and muscle activity between the bony vertebrae and soft tissue (*11*). EPs also serve as a selective permeability barrier, allowing passage of small solutes, such as nutrients, but impede transport of larger solutes, such as inflammatory factors (*12*). We have reported that cartilaginous EPs undergo chondrocyte hypertrophy and calcification during spinal degeneration, which were resorbed by osteoclasts to generate bony porous EP structure (*13*, *14*). These adaptations could also affect the mechanical properties of EPs, impair diffusion and nutrient supply (*15*), cause aberrant innervation (*16*), and result in LBP (*17*, *18*). We have recently found that osteoclasts in the cavities of the bony EP layer secrete netrin-1 (*19*). Netrin-1 promoted sensory nerve axonal outgrowth, promoted the expression of its receptor DCC (deleted in colorectal cancer) in sensory nerve and dorsal root ganglion (DRG) neurons, and induced spinal hypersensitivity in mouse models of aging and spinal instability (*19*).

Magnetic resonance imaging (MRI) studies indicate that LBP in humans is associated with structural changes of the vertebral EP (*18*, *20*). Modic changes are abnormal EP signals observed on various MRI sequences and can fluctuate over time in people with nonspecific LBP, associated more often with pain when seen with decreased T1-weighted and increased T2-weighted images, consistent with vascular granulation tissue (*21*, *22*). Histological data furthermore show that nerve density within the EP is correlated with Modic changes (*23*). Greater EP nerve density is also found in people undergoing surgery for IVD degeneration with back pain (*16*, *23*) During aging, EPs undergo ossification with elevated osteoclasts and become porous (*14*, *24*–*26*). We have demonstrated that EPs

[1]Department of Orthopaedic Surgery, Johns Hopkins University School of Medicine, Baltimore, MD 21205, USA. [2]Guangdong Provincial Key Laboratory of Orthopedics and Traumatology, Department of Spinal Surgery, First Affiliated Hospital of Sun Yat-sen University, Guangzhou 51008, P. R. China. [3]Department of Pediatrics, Johns Hopkins University School of Medicine, Baltimore, MD 21205, USA. [4]Russell H. Morgan Department of Radiology and Radiological Sciences, Johns Hopkins University School of Medicine, Baltimore, MD 21205, USA.
*Corresponding author. Email: xcao11@jhmi.edu (X.C.); zouxuen@mail.sysu.edu.cn (X.Z.)
†These authors contributed equally to this work.

in patients undergoing spinal surgery with LBP were porous with large-quantity osteoclasts and sensory innervation, whereas patients undergoing back surgery without LBP did not have porous EPs and sensory innervation (*19*). Because pain is produced by nociceptors, LBP could be caused by sensory innervation into porous EPs.

PTH regulates calcium homeostasis and bone remodeling in terrestrial vertebrates, particularly mammals (*27*). We have demonstrated that PTH regulates bone remodeling by orchestrating signaling of local factors, including transforming growth factor–β, Wnts, bone morphogenetic proteins, and insulin-like growth factor 1 (*28*–*33*). PTH (1-34) is a US Food and Drug Administration (FDA)–approved anabolic agent for the treatment of osteoporosis. We have previously shown that PTH (1-34) inhibits degradation of the extracellular matrix within IVDs, reducing disc degeneration (*34*), and attenuates osteoarthritis progression (*35*). In this study, we sought to investigate whether PTH could attenuate LBP by targeting EP sclerosis and aberrant EP sensory innervation in mouse models and a macaque model of spinal degeneration.

## RESULTS

### PTH reduced the porosity of EPs

PTH is an FDA-approved medication for the treatment of osteoporosis because PTH stimulates bone formation when given as a once-daily subcutaneous injection. Sclerotic EPs are porous, similar to osteoporotic bone. We therefore examined the impact of PTH on EP sclerosis in spine degeneration. Aged mice (72 weeks) and mice with lumbar spine instability (LSI; 8 weeks) were used as two models of spinal degeneration and injected with PTH daily for 8 weeks (Fig 1, A and B). LSI was created by resecting the L3 to L5 spinous processes along with the supraspinous and interspinous ligaments (*13*, *19*). Controls for the LSI-PTH–treated mice included sham-operated mice untreated and LSI-operated vehicle-treated mice. Controls for aged mice included aged mice injected with vehicle. Differences in EP structure were quantified by micro–computed tomography (μCT). The EPs of LSI and aged mice treated with vehicle showed increased total porosity, EP volume, and porosity volume relative to sham control (Fig. 1, C to F). The changes in EP volume and porosity were attenuated in LSI and aged mice injected with PTH (Fig 1, C to F). Although the total height of the IVD, including height of nucleus pulposus (NP) and EP, did not differ between groups, there was a shift in height, with significantly ($P < 0.05$) increased NP height and decreased EP height in LSI and aged PTH-treated mice relative to vehicle controls (Fig 1, G and H).

### PTH increased the volume of the cartilaginous EP layer and stimulated bone formation in the bony EP layer

The EP distributes intradiscal pressures onto the IVD, which is dependent on EP cartilage and bone structural properties (*36*–*39*). Histologic staining for cartilage using Safranin O/Fast Green demonstrated that the cartilaginous portion of the EP decreased in LSI and aged mice relative to sham control mice. This decrease in EP cartilage was partially attenuated by PTH treatment (Fig. 2, A to C). Tartrate-resistant acid phosphatase staining for osteoclasts and osteocalcin staining for osteoblasts were negative in the EP layer of sham-operated mice but were significantly increased in the EP pores of LSI and aged mice ($P < 0.01$; Fig. 3, A to D). PTH significantly ($P < 0.01$) increased the number of osteocalcin$^+$ osteoblasts in the cavities, and the cavities were notably smaller in the PTH groups compared with the vehicle groups (Fig. 3, C and D). Dynamic bone formation was assessed by calcein/Alizarin Red double-labeling, whereas connective tissue was visualized by Masson-Goldner trichrome staining. Normal mice did not exhibit osteosclerotic changes in the EP and, consequently, did not have any bony pores. Conversely, LSI and aged mice displayed osteosclerotic EP changes, with increased osteoclastic activity and porous cavity enlargement. This process results in the substitution of old bone (calcein green) with new bone (Alizarin Red), leading to the exclusive presence of the red color (fig. S1, A and B). PTH-injected LSI and aged mice had stimulation of bone formation with smaller pores in the sclerotic EP, as demonstrated by double labeling noted in the pores and osteoid deposition relative to vehicle-injected LSI and aged controls (fig. S1, A and B). Type H blood vessels, defined by high staining intensity of both CD31 and endomucin (EMCN), are specifically coupled with bone formation (*40*, *41*). Immunofluorescence costaining of CD31 and EMCN showed that type H blood vessels were significantly ($P < 0.01$) increased in the EP cavities of PTH-injected LSI and aged mice, further indicating PTH-induced anabolic bone formation in the pores (Fig. 3, E and F).

### PTH improved the mechanical properties of EPs

To investigate whether the change in porosity affected EP mechanical properties, finite element analysis based on CT data was performed, which measured displacement ($U$) magnitude and von Mises stress (Mises stress) as a way to evaluate the deformation and stress distribution of EP. The EPs of sham-operated controls experienced the lowest stress, whereas the highest stress occurred in the larger cavities of porous EPs in both LSI and aged mice with vehicle treatment (Fig. 3, G and H). PTH significantly reduced the stress in LSI and aged mice compared with the vehicle group ($P < 0.01$; Fig. 3, G and H). Together, PTH induced bone formation and reduced the porosity of EPs, decreasing mechanical stress in both LSI and aged mouse models of spinal degeneration.

### PTH reduced sensory nerve innervation in porous EPs

We have recently reported that aberrant innervation in EP pores results in increased prostaglandin E2 ($PGE_2$) concentrations that mediate spinal hypersensitivity or mechanical allodynia during spinal degeneration (*19*). Because PTH reduced bony EP porosity, we next investigated the effect of PTH on sensory innervation. We confirmed our prior report by immunostaining spine sections and showed that the expression of protein gene product 9.5 (PGP9.5), a marker broadly expressed on nerve fibers, was increased in the EPs of LSI and aged mice relative to those of sham controls, in which PGP9.5 was undetectable (Fig. 4, A to C). PTH significantly reduced PGP9.5$^+$ nerve fibers in the EPs of LSI and aged mice relative to vehicle controls ($P < 0.01$; Fig. 4, B and C), whereas PGP9.5$^+$ nerve fibers in the annulus fibrosus remained unchanged among all treatment groups (Fig. 4, B and D). COX-2 by immunostaining (Fig. 4E) and $PGE_2$ by enzyme-linked immunosorbent assay (ELISA) were increased in the EPs of LSI and aged mice relative to sham control, similar to our prior report (*19*), and PTH treatment decreased the concentrations of inflammatory factors COX-2 and $PGE_2$ relative to vehicle controls (Fig. 4, E to G). Analysis of EP mRNA also demonstrated that PTH decreased *Ptgs2* (fig. S2).

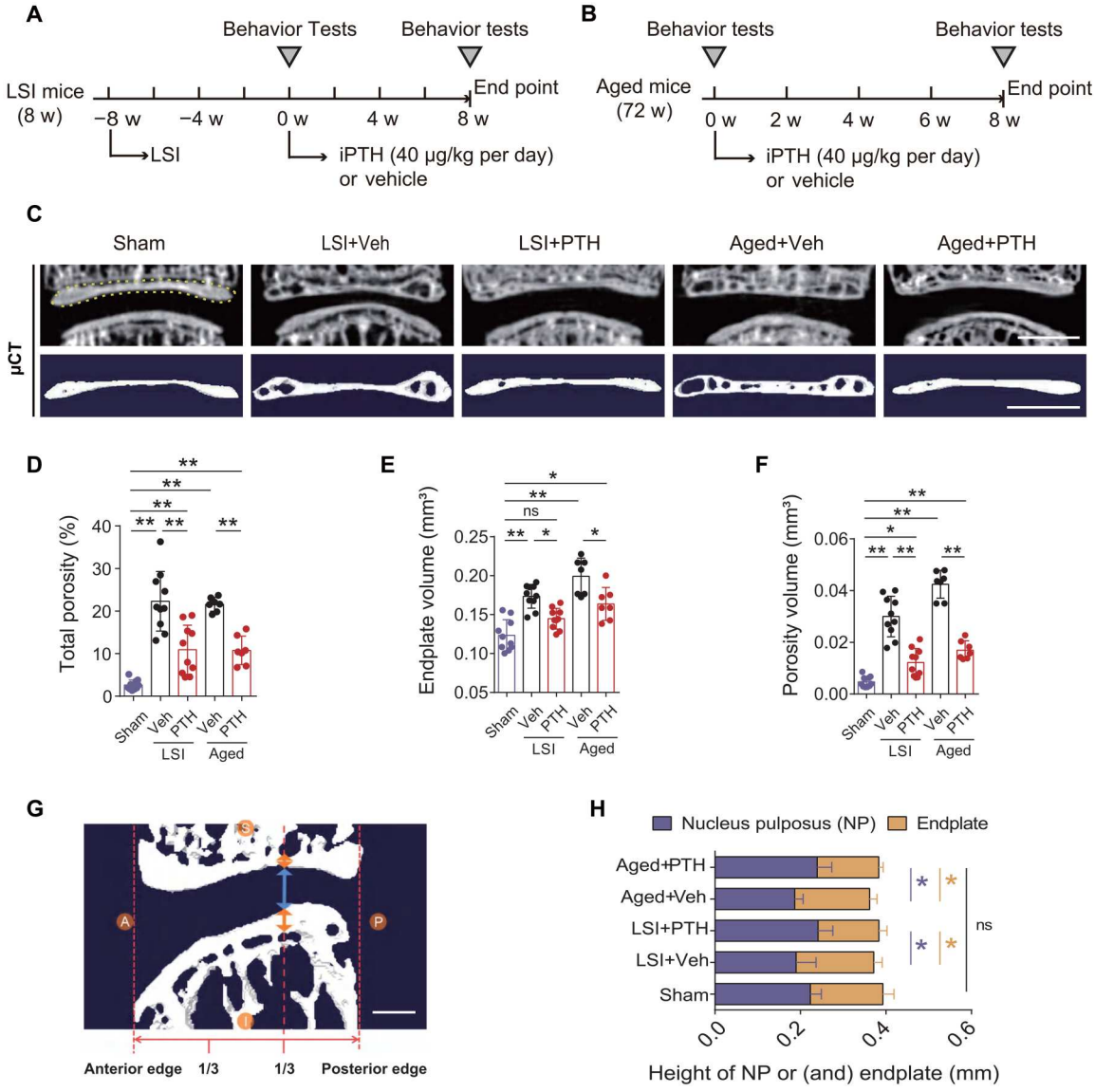


**Fig. 1. PTH ameliorated EP remodeling in two mouse models of spinal degeneration.** (**A** and **B**) Schematic diagram of the procedure surgery and PTH treatment of LSI (A) and aged mice (B). (**C**) Representative coronal high-resolution μCT images (top) and three-dimensional images (bottom) of L4/5 EPs in sham-operated mice and LSI or aged mice treated with PTH or vehicle (Veh). Scale bars, 0.5 mm. The yellow dotted line area represents the EP. (**D** to **F**) Quantitative analysis of total porosity (D), EP volume (E), and porosity volume (F) of the mouse L4/5 EP. (**G**) Representative sagittal high-resolution μCT image of a L4/5 EP from a sham-operated mouse. The blue arrow indicates height of NP; the yellow arrow indicates height of EP (P, posterior; A, anterior; S, superior; I, inferior; scale bars, 0.2 mm). (**H**) Quantification of NP height, EP thickness, and total height of the IVD (NP and EP) in the posterior one-third of L4-L5 in the sagittal plane. $n = 10$ (Sham, LSI model) or $n = 7$ (aged model) per group. All data are shown as means ± SD. Statistical significance was determined by one-way ANOVA and Student's $t$ test. $^*P < 0.05$ and $^{**}P < 0.01$. ns, no significant difference.

To determine the origins of EP innervation, a retrograde nerve tracing experiment was conducted in which Dil was injected into the L4-L5 EP. Immunofluorescence analysis showed that Dil-positive and PGP9.5-positive neurons were highly abundant in the DRGs of LSI and aged-mice injected with vehicle relative to sham, and PTH decreased the aberrant innervation in LSI and aged mice (Fig. 5A). To further classify nerve fiber type, coimmunofluorescence staining with PGP9.5, calcitonin gene–related peptide (CGRP), neurofilament 200 (NF200), Piezo-type mechanosensitive ion channel component 2 (PIEZO2), isolectin B4 (IB4), and P2X purinoceptor 3 (P2X3) with Dil was performed. Dil-positive neurons were positive for CGRP, NF200, and PIEZO2 but not IB4 or P2X3. There was no statistically significant difference in the percentage of copositive Dil and CGRP, NF200, or PIEZO2 DRG neurons between LSI and aged mice injected with either vehicle or PTH ($P > 0.05$; Fig. 5, B and C). Overall, PTH-induced bone formation reduced the porosity of EPs and nonspecifically reduced sensory innervation of EP cavities in LSI and aged mice.

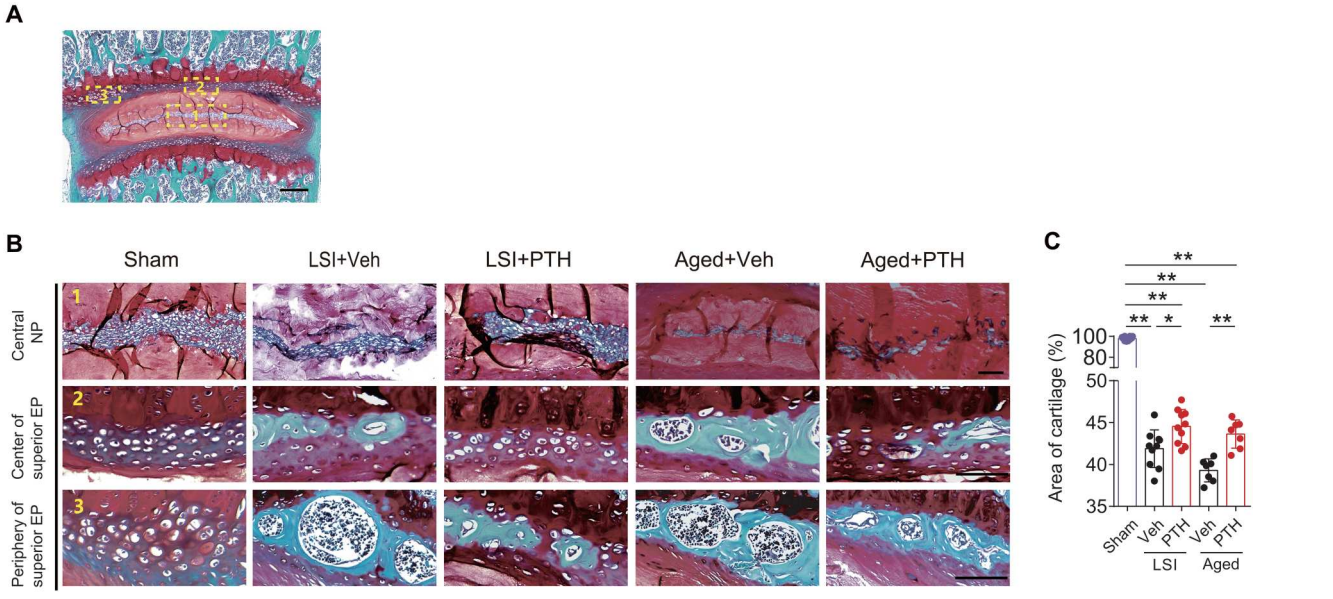


**Fig. 2. Cartilage EP degeneration was attenuated by PTH.** (**A**) Representative images of a L4-L5 coronal EP from a sham-operated mouse stained for Safranin O (red, for proteoglycans) and Fast Green (green, for bony cavities). Scale bars, 100 μm. 1, 2, and 3 represent central nucleus pulposus, center, and periphery of superior EP, respectively. (**B**) Magnified sections of L4-L5 coronal EPs containing the central nucleus pulposus (NP) (1), the center of the superior EP (2), and the periphery of the superior EP (3) from sham-operated mice and LSI or aged mice treated with PTH or vehicle (Veh). (**C**) Quantitative analysis of the area of cartilage in the whole EP based on Safranin O and Fast Green staining. $n = 10$ (Sham, LSI model) or $n = 7$ (aged model) per group. All data are shown as means ± SD. Statistical significance was determined by one-way ANOVA and Student's $t$ test. $^*P < 0.05$ and $^{**}P < 0.01$ compared with sham or vehicle group.

### PTH attenuated LBP-related behavior in mice

We then assessed pain-related behaviors in LSI and aged mice to examine the potential effects of PTH on LBP. Hyperalgesia tests of pressure tolerance were performed to measure spinal hypersensitivity after development of spinal degeneration at 0 weeks and after 8 weeks of vehicle or PTH daily injections [see Fig. 1 (A and B)]. Pressure tolerance decreased significantly ($P < 0.05$) after LSI surgery relative to that of sham-operated mice (Fig. 6A), indicating the development of low back pressure hyperalgesia. There was no change in pressure tolerance in LSI mice after vehicle treatment, whereas PTH treatment resulted in increased pressure tolerance (Fig. 6A), indicating that this form of hyperalgesia was attenuated with PTH. We also measured spontaneous activity as time spent running on exercise wheels per 24 hours. Distance traveled, active time, and maximum speed were decreased significantly at 0-weeks in LSI surgery relative to that of sham-operated mice ($P < 0.05$; Fig. 6, B to D). After 8 weeks, vehicle injections had no effect on spontaneous activity, whereas PTH injections increased the distance traveled (Fig. 6B), active time (Fig. 6C), and maximum speed (Fig. 6D) relative to 0 weeks and were not statistically different from spontaneous activity of sham controls. In parallel, we evaluated the effects of PTH on LBP in aged mice (Fig. 6, E to H). Similarly, PTH treatment increased pressure tolerance (Fig. 6E) and spontaneous activity (Fig. 6, F to H) in 72-week-old mice relative to baseline. These results suggest that PTH attenuates pain-related behaviors in LSI and aged mouse models.

### PTH analgesia mechanism was independent of IVD pathology

Aberrant innervation within the EP and the nucleus pulposus has been associated with nonspecific LBP (*42*). To discern whether the analgesic effect of PTH treatment is due to signaling within the nucleus pulposus of IVD, we disrupted PTH signaling within the IVD by crossing Notochordal-Cre mice with $Pth1r^{f/f}$ mice ($Pth1r^{-/-}$). PTH1R staining of the degenerated spines of these mice demonstrated PTH1R expression in osteoblasts and osteocytes of the vertebral body and EPs (fig. S3A). After 8 weeks of PTH treatment, similar to our previous report (*34*), μCT showed that the increase in IVD height caused by PTH treatment in aged $Pth1r^{+/+}$ mice was abolished in $Pth1r^{-/-}$ mice (fig. S3, B to E). However, the EPs of $Pth1r^{-/-}$ aged mice remained responsive to PTH, showing decreased EP volume and height (Fig. 7, A and B, and fig. S3C), total porosity (Fig. 7C), and porosity volume (Fig. 7D) relative to vehicle control. Histological staining of the EP with Safranin O/Fast Green demonstrated that PTH treatment decreased EP porosity in $Pth1r^{-/-}$ aged mice and in $Pth1r^{+/+}$ mice (Fig. 7, E and F). Immunofluorescence staining showed that protein expression of PGP9.5 decreased in EP nerve fibers in both PTH-treated $Pth1r^{-/-}$ aged mice and $Pth1r^{+/+}$ controls (Fig. 7, G and H). Regarding pain behavior, PTH treatment significantly ($P < 0.05$) increased pressure tolerance (Fig. 7I), distance traveled (Fig. 7J), and active time (Fig. 7K) in $Pth1r^{-/-}$ aged mice and $Pth1r^{+/+}$ mice relative to baseline. PTH treatment did not significantly change maximum speed ($P > 0.05$; Fig. 7L). Together, these results suggest that PTH-mediated improvement in pain-related behaviors and aberrant spinal innervation are independent of PTH signaling in the nucleus pulposus of IVD, further implicating an important role for EPs in nonspecific LBP.

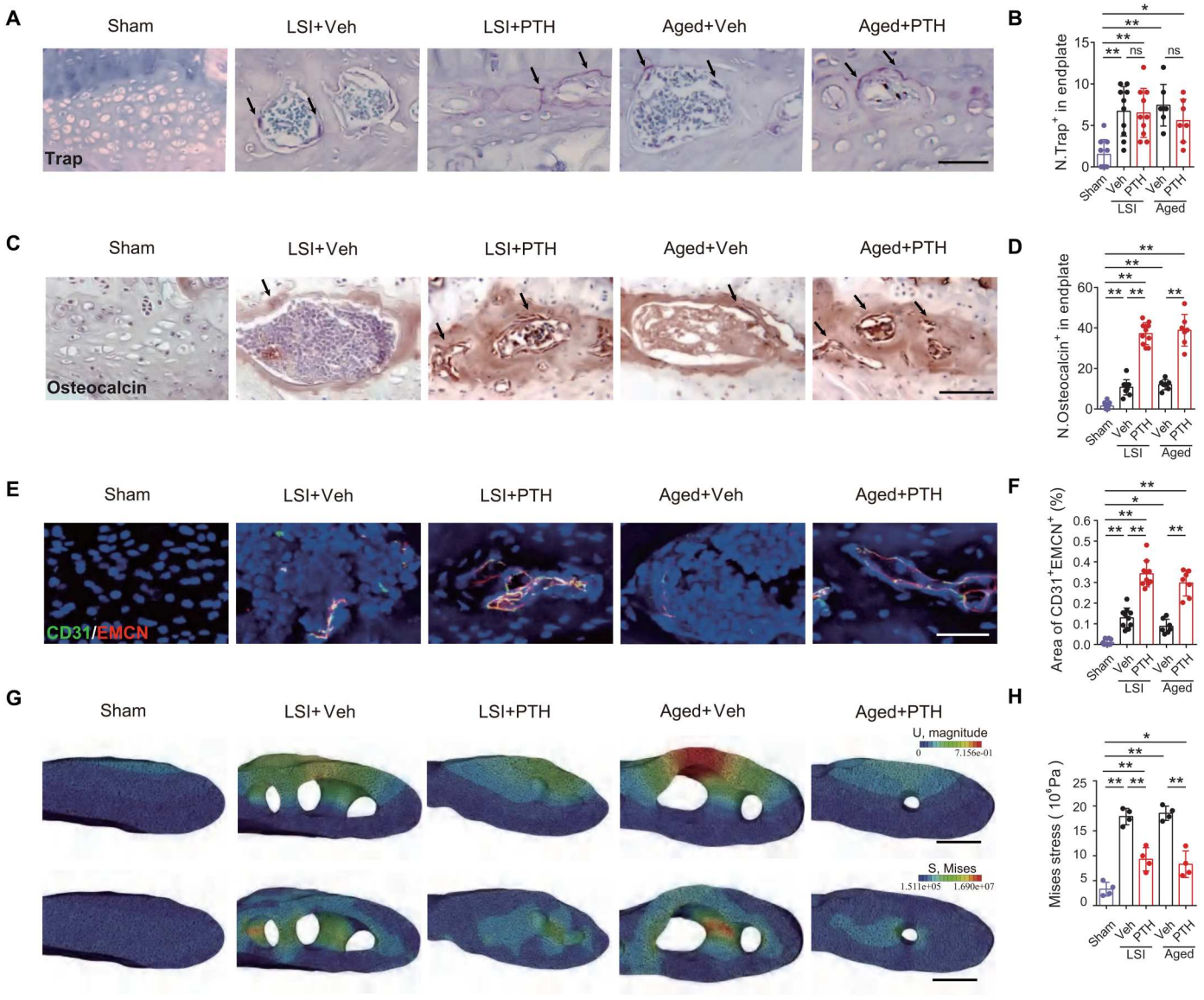


**Fig. 3. PTH induced osteogenesis and angiogenesis in bony EP.** (**A** to **F**) Representative images and quantitative analysis of the number of positive cells in L4-L5 EP coronal sections from sham-operated mice and LSI or aged mice treated with PTH or vehicle (Veh). $n = 10$ (Sham, LSI mice) or $n = 7$ (aged mice) per group. (A and B) Tartrate resistance acid phosphatase (Trap) (magenta) staining. Scale bar, 100 μm. (C and D) Osteocalcin immunostaining. Scale bar, 100 μm. (E and F) CD31 (green) and endomucin (EMCN) (red) immunofluorescence staining. DAPI (4′,6-diamidino-2-phenylindole) stains nuclei blue. Scale bar, 50 μm. (**G** and **H**) Representative images of finite element analysis in L4-L5 superior EPs, including *U* magnitude (G, top) and Mises stress (G, bottom, and H) to evaluate the deformation and stress distribution of EP for all treatment groups, Scale bars, 100 μm. $n = 4$ per group. All data are shown as means ± SD. Statistical significance was determined by one-way ANOVA and Student's *t* test. $^{*}P < 0.05$ and $^{**}P < 0.01$.

## PTH improved IVD degeneration and decreased EP porosity and innervation in aged rhesus macaques

Given the concerns of translatability of mouse findings to humans, we next investigated the effect of PTH on spinal degeneration in rhesus macaques. Rhesus macaques, similar to humans, are bipedal and show evidence of spinal degeneration with aging. Male and female rhesus macaques (14 to 17 years old) were screened radiographically for IVD degeneration based on Pfirrmann score, a radiographic score of IVD degeneration used in human degenerative IVD disease studies (fig. S4A) (*43*). Macaques with grades 2 to 4 of the lower lumbar spine (L4-L5, L5-L6, and L6-L7 IVDs) were randomized and injected with vehicle or PTH (10 μg/kg per day) for 3 months (fig. S4B). At baseline, the vehicle group had a higher proportion of males (three versus two) and thus had a greater mean weight relative to PTH group (table S1). At baseline, there was no difference in serum bone turnover markers (N-terminal propeptide of type 1 procollagen, beta C-terminal telopeptide, and osteocalcin) or in bone mineralization (alkaline phosphatase, calcium, and phosphate) between vehicle and PTH groups. Spinal degeneration of all seven lumbar IVDs of each macaque was assessed by MRI, including grading of Pfirrmann score, as well as T1ρ (T1 rho) and T2 map signal intensity measured on quantitative

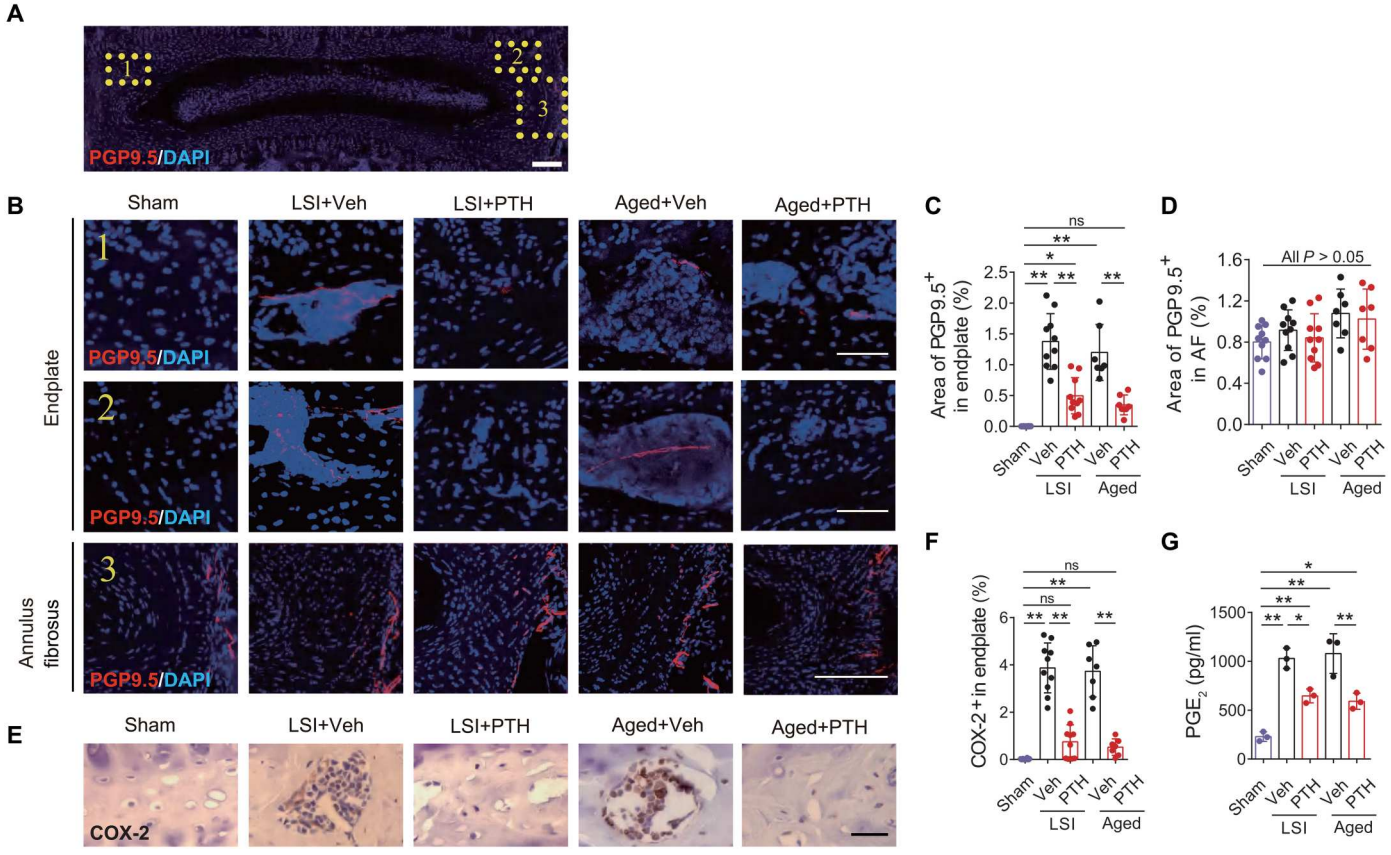


**Fig. 4. PTH reduced sensory nerve innervation in EPs.** (**A**) Representative low-magnification immunofluorescence image of a L4-L5 EP coronal section from a sham-operated mouse stained for PGP9.5$^+$ (red) sensory nerve fibers and DAPI (stains nuclei blue) (scale bar, 100 μm). Yellow rectangles denote areas of higher-magnification images in (B). (**B**) Representative immunofluorescence images of L4-L5 EP coronal sections from sham-operated mice and LSI or aged mice treated with PTH or vehicle (Veh) for stainings as in (A) (1 and 2) EPs (scale bars, 50 μm) and (3) annulus fibrosus (scale bar, 100 μm). (**C** and **D**) Quantitative analysis of the percentage of PGP9.5$^+$ area in EP (C) or annulus fibrosus (AF) (D). $n = 10$ (Sham, LSI mice) or $n = 7$ (aged mice) per group. (**E** and **F**) Immunohistochemical staining (E) and quantitative analysis (F) of COX-2 (brown) in L4-L5 EPs. Hematoxylin stains nuclei purple. (**G**) ELISA analysis of prostaglandin $E_2$ ($PGE_2$) concentration in lysate of lumbar EPs. $n = 3$ per group. All data are shown as means ± SD. Statistical significance was determined by one-way ANOVA and Student's $t$ test. *$P < 0.05$ and **$P < 0.01$.

MRI to analyze the degree of IVD degeneration. There were statistically significant differences in IVD degeneration at baseline of all imaging parameters, with the PTH group showing more severe lumbar IVD degeneration [lower T1ρ ($P = 0.032$) and T2 signal intensity ($P = 0.012$) and higher Pfirrmann grade ($P = 0.044$)] relative to vehicle group (table S1). There was no difference in IVD degeneration at specific lumbar segments (table S2).

After 3 months of vehicle or PTH injection, the PTH group trended to lower Pfirrmann scores relative to vehicle (table S1) but did not reach statistical significance using a logistic multilevel mixed-effect regression model ($P = 0.102$; table S3). Signal intensity of both T1ρ and T2 map increased in the PTH group, whereas these parameters decreased in vehicle-treated macaques (table S1 and fig. S2C). Overall, PTH treatment significantly improved T1ρ ($P = 0.011$) and T2 map ($P = 0.018$) signal intensity relative to vehicle, as assessed by a linear multilevel mixed-effect regression model (table S3). Bone turnover markers in serum increased with PTH relative to vehicle after 3 months (table S1). μCT analysis revealed that PTH treatment decreased EP volume, total porosity, and porosity volume (Fig. 8, A to D) relative to the vehicle group, similar to the PTH treatment effects seen in aged mice. Histological staining with Safranin O/Fast Green furthermore showed that PTH treatment increased EP cartilage matrix area (Fig. 8, E and F). Immunofluorescence staining showed significantly decreased PGP9.5 and COX-2 expression in the EPs of the PTH group relative to the vehicle group ($P < 0.01$; Fig. 8, G to J).

## DISCUSSION

LBP profoundly affects quality of life and daily physical activity, especially in the elderly population, increasing risk of frailty. Current treatments involve either analgesics (*44*) or surgeries such as disc arthroplasty, spinal fusion, or disc decompression to address structural abnormalities, which only improve pain in some of the affected patients (*45*, *46*). There is no disease-modifying medication to protect the spine from accelerated degeneration nor any medication specific for LBP. There have been multiple studies analyzing the impact of PTH on back pain. Nevitt *et al.* (*47*) published a meta-analysis in 2005 demonstrating that postmenopausal women or men with idiopathic or hypogonadal osteoporosis had a reduced risk of back pain when treated with PTH relative to placebo. Eastman *et al.* (*48*) more recently published a meta-analysis on

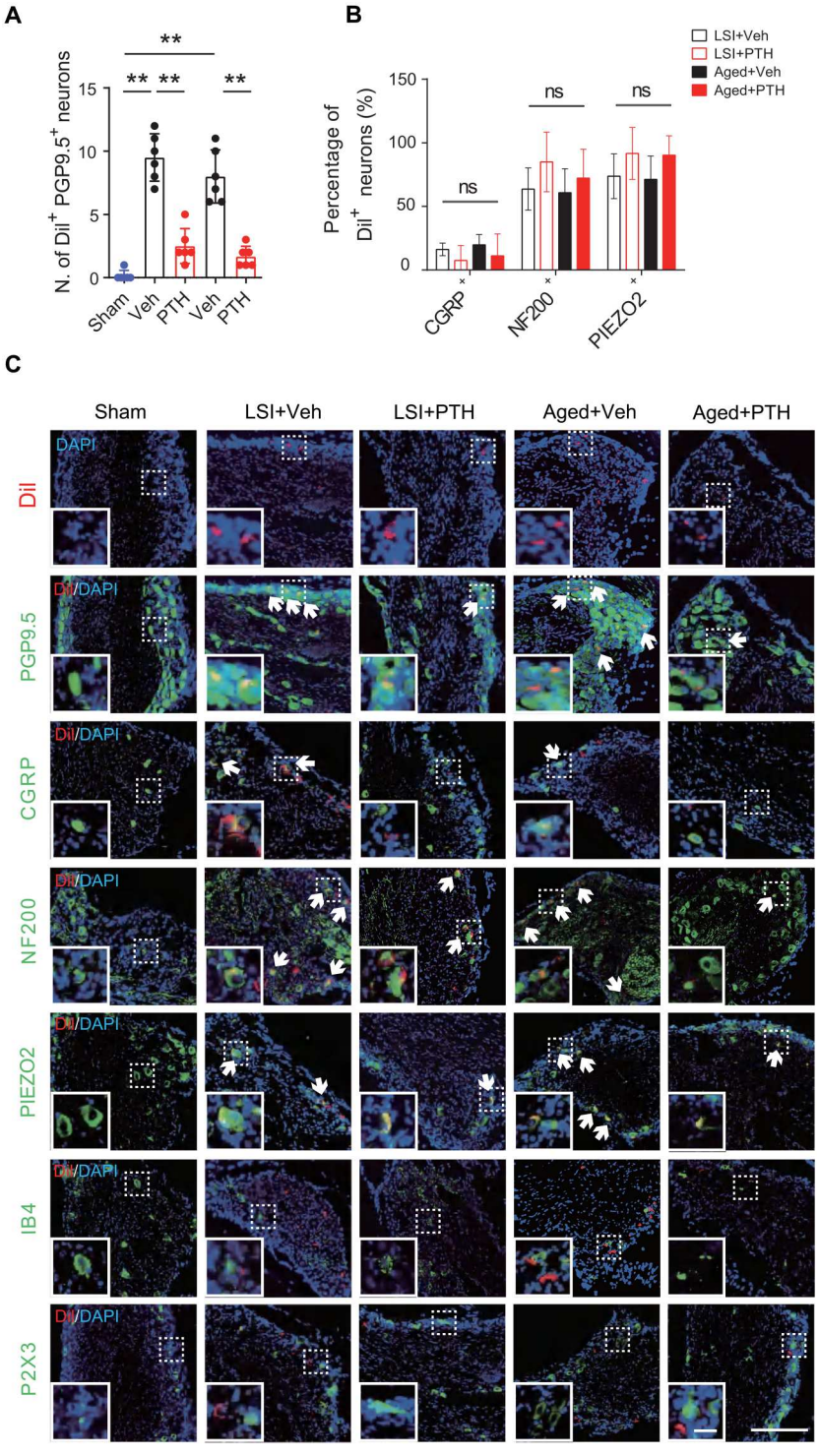


**Fig. 5. PTH reduced sensory nerve innervation from the DRG.** (**A**) Quantitative analysis of the number of Dil-positive and PGP9.5-positive DRG neurons. (**B**) Quantitative analysis of the percentage of Dil-positive (red) DRG neurons that are also CGRP, NF200, and PIEZO2 positive. (**C**) Representative immunofluorescence images of DRG sections (including local 2.5× magnification images) stained for Dil (red, top row) and PGP9.5, CGRP, NF200, PIEZO2, IB4, and P2X3 (green). Copositive cells positive for both appear yellow. Scale bars, 200 μm. $n = 6$ (Sham, LSI mice) or $n = 6$ (aged mice) per group. All data are shown as means ± SD. Statistical significance was determined by one-way ANOVA and Student's $t$ test. $^{**}P < 0.01$.

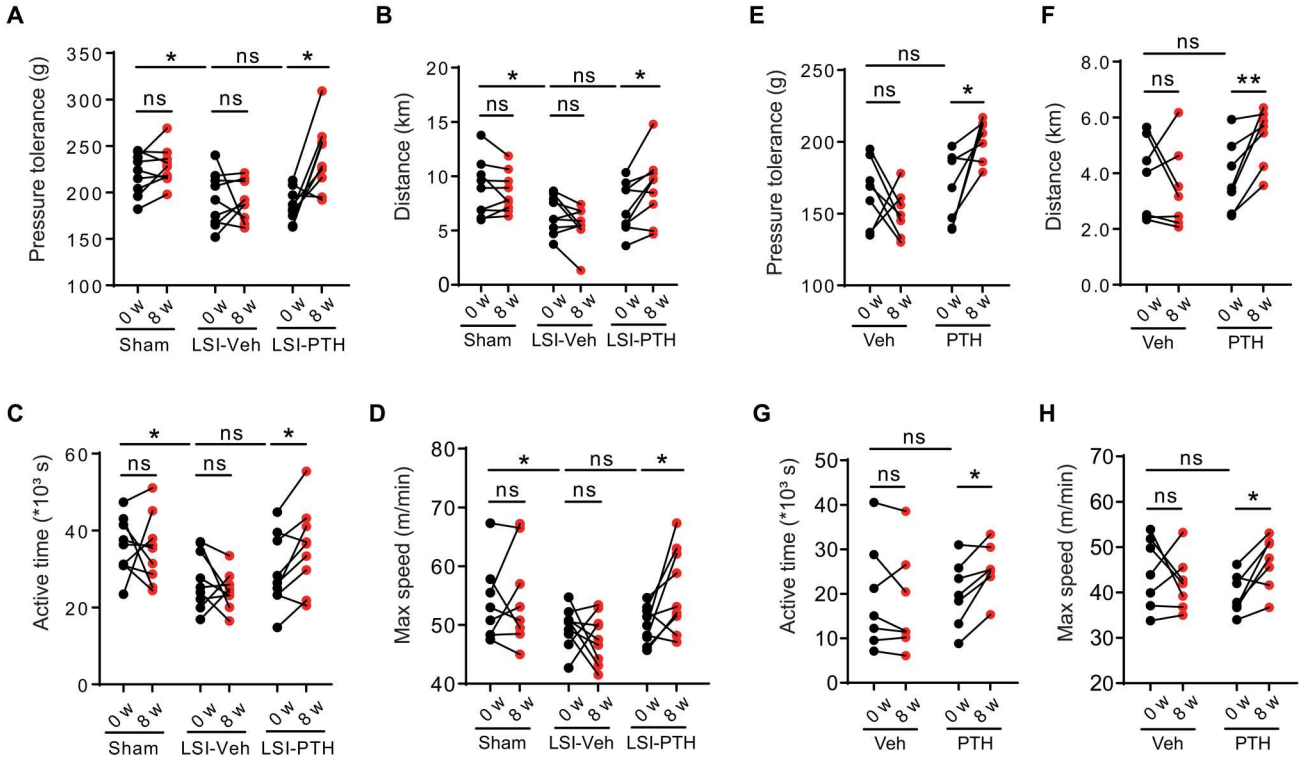


**Fig. 6. PTH attenuated LBP-related behaviors in LSI and aged mice.** (**A** to **D**) Longitudinal comparison of LBP treatment effects in LSI mice. Data from sham-operated and LSI mice treated with PTH or vehicle (Veh) are shown. (A) Quantification of pressure tolerance in response to mechanical stimulation above L4-L5. (B) Distance traveled, (C) active time, and (D) maximum speed on the wheel per 24 hours. $n = 9$ (Sham, LSI model) or $n = 7$. (**E** to **H**) Longitudinal comparison of treatment effects (as in A to D) for aged mice. Aged mice treated with PTH or vehicle (Veh) are shown. Statistical significance was determined by one-way ANOVA and Student's *t* test. All data are shown as each individual mouse. $^*P < 0.05$ and $^{**}P < 0.01$.

the effects of PTH on fracture healing and pain. Of the eight trials that reported pain outcomes, self-reported functional scores were improved in 50% of the trials, and by meta-analysis, 38% had improvement in pain relative to controls. The controls in these studies varied from either placebo or other standard of care, such as vertebroplasty, which was also associated with pain improvement (*48*). Overall, these studies suggest that there is a subset of patients showing improvement of LBP with PTH treatment. We have previously shown that PTH can ameliorate IVD degeneration by signaling in the nucleus pulposus of the IVD (*34*). In the current study, we show that PTH also improved EP sclerosis. We confirmed prior reports of aberrant EP innervation with bone marrow expansion in spine degeneration (*16*), which was reduced in PTH-treated groups. Pain tolerance and spontaneous running on activity wheels improved in both mouse models of spinal degeneration treated with PTH. To increase the translational impact of our work, we also validated our findings in aged rhesus macaques, noting improvement in an MRI radiological outcome measure of IVD degeneration.

Nonspecific LBP has multiple etiologies and is commonly associated with IVD degeneration (*49*). IVD degeneration is caused largely by aging (*50*) but may also result from degenerative changes in other spinal structures. The spine is a complex, amphiarthrodial joint, consisting of alternating bony vertebrae and fibrocartilaginous IVDs. The IVD is composed of a central nucleus pulposus, a peripheral annulus fibrosus, and, superiorly and inferiorly, two cartilaginous EPs. Normally, sensory nerves are not present in nucleus pulposus and cartilaginous EPs, whereas chemokine-induced sensory innervation and capillary growth has been observed after annulus fibrosus rupture (*51*, *52*). Given that annulus fibrosus rupture results in disc herniation and may also cause compression of the adjacent nerve root, this would not be an example of nonspecific LBP because this phenomenon is easily identified on MRI. In our mouse models of spinal degeneration, we noted the presence of sensory nerves in both the annulus fibrosus and EP without annulus fibrosus rupture. However, only sensory innervation of the EP was reduced by PTH, coinciding with the improvement in pain-hypersensitivity behaviors. We have previously shown that PTH could rejuvenate the degenerated IVD via direct signaling in the IVD (*34*) but had not examined pain behaviors. In the current study, knockout of *Pth1r* in notochordal cells showed continued sensitivity to PTH effects on EP structure and LBP-related behaviors. Our results support the hypothesis that sensory innervation within the EP, rather than nucleus pulposus and annulus fibrosus, is a major contributor to nonspecific LBP.

EPs transmit mechanical loads from body weight and muscle activity between the bony vertebrae and soft tissue; thus, the thickness, porosity, and curvature are important structural determinants of EP function (*36*–*39*). During aging and spinal degeneration, EP chondrocytes hypertrophy with thinning of cartilage and gradual ossification with expansion of the bony porous EP (*14*, *25*, *26*, *53*, *54*). EP sclerosis is associated with changes in EP mechanical properties,

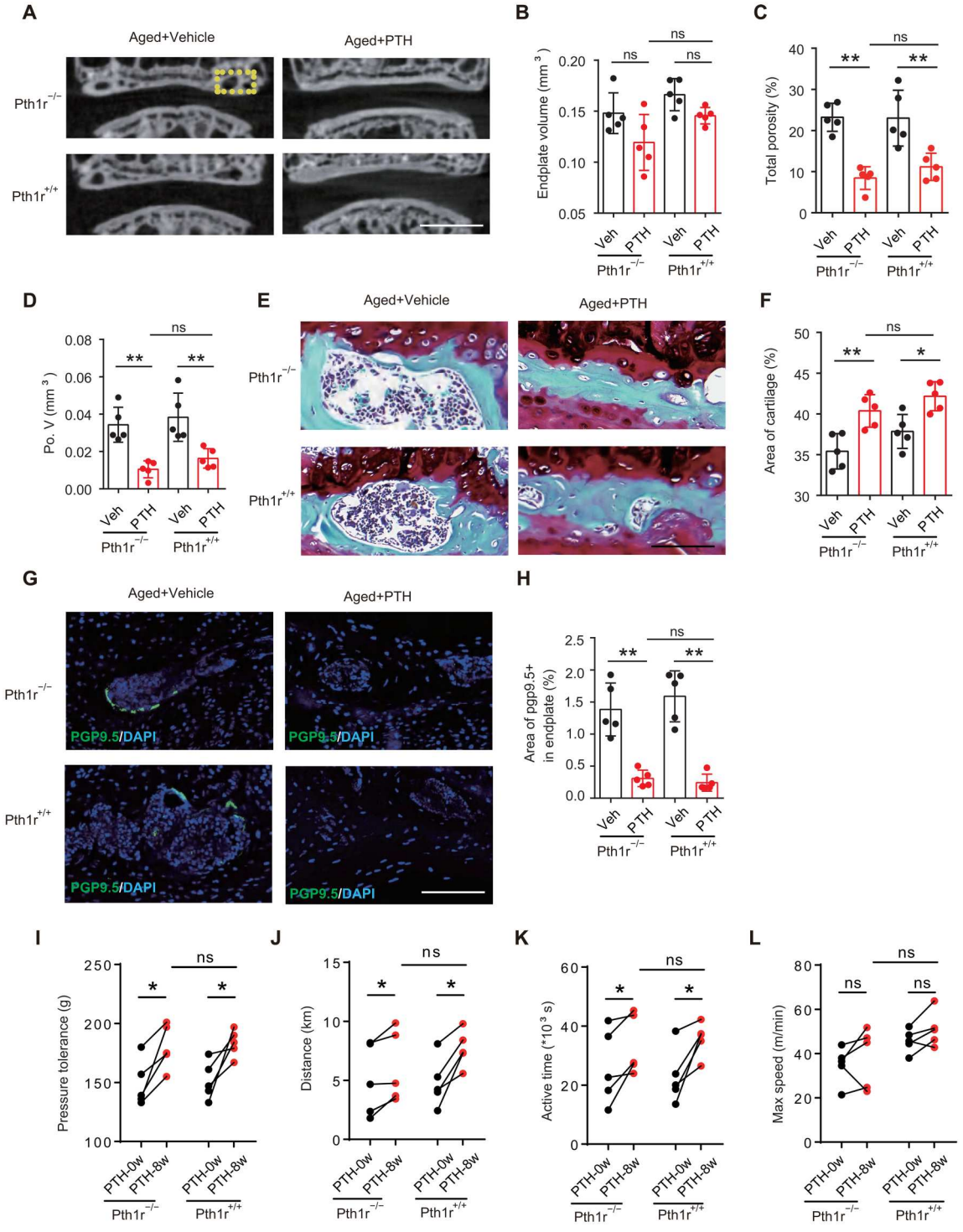


**Fig. 7. PTH-mediated improvement in pain behaviors is independent of PTH signaling within the nucleus pulposus.** (**A**) Representative coronal high-resolution μCT images of L4-L5 EPs from aged mice with conditional knockout of the PTH type 1 receptor in the nucleus pulposus (*Pth1r*$^{-/-}$) and aged *Pth1r*$^{+/+}$ mice treated with PTH or vehicle (Veh). Scale bar, 0.5 mm. (**B** to **D**) Quantitative analysis of EP volume (B), total porosity (C), and porosity volume (D) in *Pth1r*$^{-/-}$ and *Pth1r*$^{+/+}$ aged mice treated with PTH or vehicle (Veh). (**E**) Representative coronal L4-L5 EP images of Safranin O and Fast Green staining for mice as described in (A). Proteoglycan is in red, and bony cavities are in green. Scale bar, 100 μm. (**F**) Quantitative analysis of the area of cartilage in the whole EP based on Safranin O and Fast Green staining. $n = 5$ per group. (**G**) Representative coronal immunofluorescence images of L4-L5 EPs stained for PGP9.5$^{+}$ (green) nerve fibers for mice as described in (A). Scale bar, 100 μm. (**H**) Quantitative analysis of PGP9.5-positive area in *Pth1r*$^{-/-}$ and *Pth1r*$^{+/+}$ aged mice treated with PTH or vehicle (Veh). (**I** to **L**) Change in pressure tolerance (I) and spontaneous activity as measured by distance traveled (J), active time (K), and maximum speed (L) on running wheel per 24 hours in *Pth1r*$^{-/-}$ and *Pth1r*$^{+/+}$ aged mice treated with PTH. $n = 5$ per group. All data are shown as each individual mouse. Statistical significance was determined by one-way ANOVA and Student's *t* test. $^{*}P < 0.05$ and $^{**}P < 0.01$.

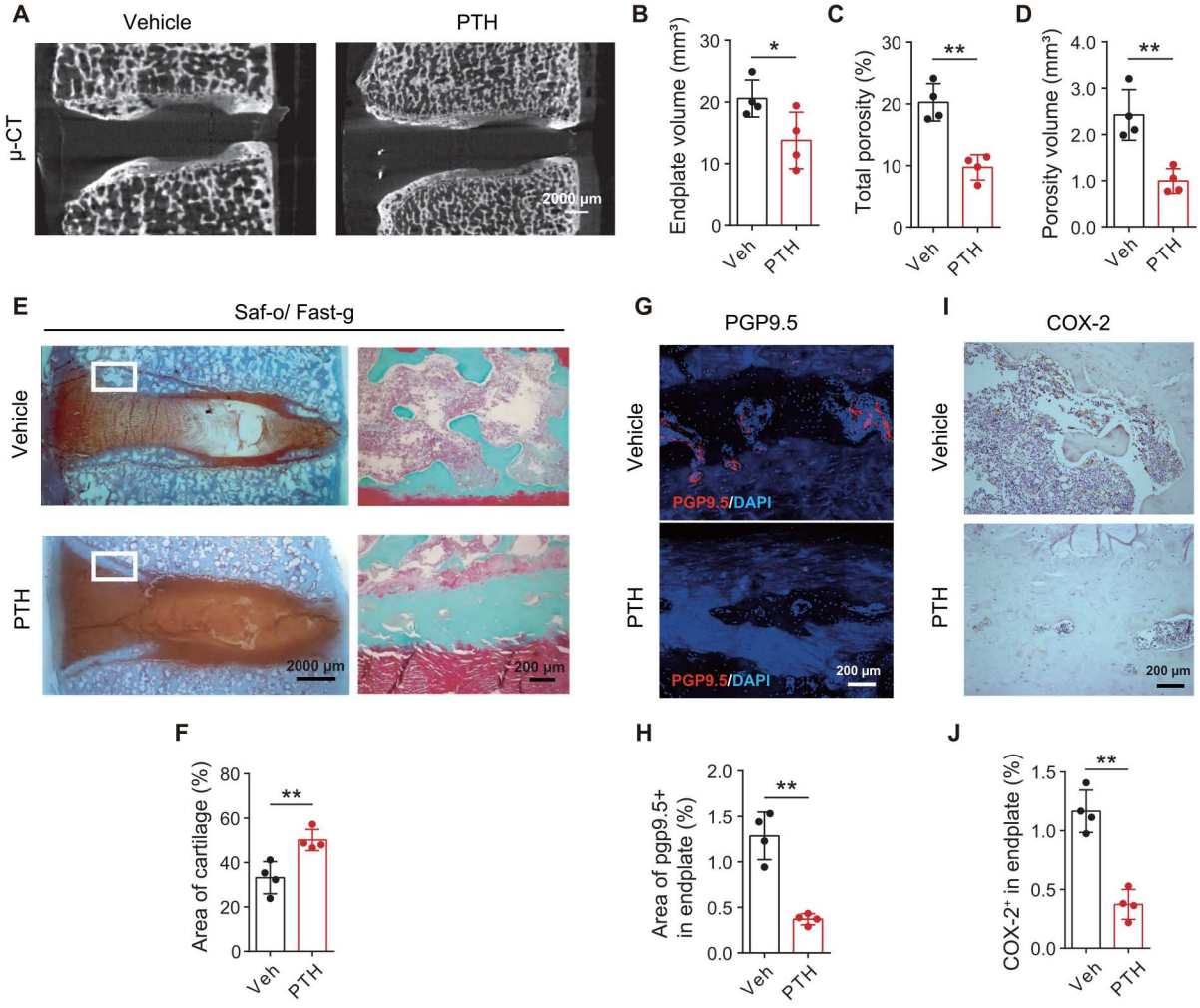


**Fig. 8. PTH improved IVD degeneration and decreased EP porosity and innervation in aged rhesus macaques.** (**A**) Representative sagittal high-resolution μCT images of the lumbar vertebrae (L4-L5) in aged rhesus macaque after 3 months of PTH or vehicle (Veh) treatment. Scale bar, 2000 μm (**B** to **D**) Quantitative analysis of EP volume (B), total porosity (C), and porosity volume (D) in the lumbar EP. $n = 4$ per group. (**E**) Representative coronal L4-L5 EPs of Safranin O and Fast Green (Saf-O/Fast G) staining in macaques after 3 months of PTH or vehicle (Veh). (**F**) Quantitative analysis of percentage of cartilage area in the lumbar EP. $n = 4$ per group. (**G**) Representative coronal immunofluorescence images of L4-L5 EPs stained for PGP9.5 (red) nerve fibers and DAPI (blue) staining of nuclei in macaques as described in (E). Scale bars, 200 μm. (**H**) Quantitative analysis of PGP9-positive area in the lumbar EP. $n = 4$ per group. (**I**) Representative coronal immunohistochemical images of L4-L5 EPs stained for COX-2 (brown) in macaques as described in (E). Scale bar, 200 μm. (**J**) Quantitative analysis of percentage of COX-2–positive area in the lumbar EP. $n = 4$ per group. Statistical significance was determined by Student's $t$ test. All data are shown as means ± SD. $^*P < 0.05$ and $^{**}P < 0.01$ compared with the vehicle-treated group.

such as calcifications, which are thought to disrupt diffusion of nutrients and hydration to the IVD and may contribute to IVD degeneration (*55*). In people with LBP, EP sclerosis is observed (*10*, *16*, *17*), as well as increased nerve density in the EP (*18*). Nerve density is greatest in EPs from people with Modic type 1 or 2 changes relative to patients with normal EP on MRI (*23*). PTH stimulates bone remodeling by modulating the bone marrow microenvironment through the orchestration of signaling of local factors (*28*). We found that PTH-stimulated osteoblast bone formation reduced EP porosity and reduced EP volume. PTH is also known to promote chondroregeneration (*56*). We observed expansion of the cartilage EP with PTH. The change in EP morphology correlated with an increase in IVD volume. Because angiogenesis is coupled with osteogenesis, we also evaluated the impact of PTH on EP vasculature, noting an increase in type H blood vessels with PTH. Further studies are necessary to conclude whether the increase in type H vessels improves nutrient diffusion. Together, the impact of PTH on the EP structure resulted in improvement in EP mechanical properties with less von Mises stress.

We previously found that abnormal mechanical stress caused by LSI increases the activity of osteoclasts and osteoclast secretion of Netrin-1, leading to aberrant EP sensory innervation (*19*). Prostanoids, specifically $PGE_2$, regulate inflammation and sensitize neurons to pain. In this study, aberrant sensory innervation of EPs was noted, and the protein expression of $PGE_2$ and COX-2 in the EP with osteosclerosis were increased, consistent with results in long bone (*57*). In addition, we observed changes in behavior suggestive of pain hypersensitivity. Eight weeks of daily PTH administration reduced EP innervation and $PGE_2$ and COX-2 concentrations. The finding that PTH reduced $PGE_2$ and COX-2

in osteoblasts is contrary to prior reports that PTH stimulates the expression of $PGE_2$ in osteoblasts in vitro (*58*, *59*). A possible explanation is that the effect of PTH on $PGE_2$ in vivo is indirect. Tracing of neurons to the DRG revealed that the decrease in sensory innervation was nonspecific. Further studies are necessary to understand the mechanism of PTH reduction of $PGE_2$ and how nerve fibers decreased.

There are limitations to our study. We were unable to investigate the behavior of aged rhesus macaques to determine whether there was a change in behavior due to the lack of reliable behavioral testing methods for this species. Second, although PTH improved pain, the duration of effect is unknown. PTH reduces porosity of EPs to relieve pain, and it also attenuates spine degeneration in aging and LSI mice (*34*). After termination of PTH treatment, the therapeutic effects should be maintained for some time in aged mice but with mechanical instability, such as in the LSI model; without correction of the underlying defect, the disease may recur. Longer observation after cessation of PTH would be needed to investigate this remaining question. A third limitation is that PTH treatment effects on MRI outcome measures were inconclusive. Mice MRI were not evaluated in this study, and the number of rhesus macaques used was not sufficient to show definitive evidence of improvement in IVD degeneration by Pfirrmann grade, a radiographic score of IVD degeneration used in human degenerative IVD disease studies (*43*). However, T1ρ and T2 map did increase in PTH-treated macaques relative to the vehicle-treated controls, demonstrating a potential radiographic biomarker for future clinical studies.

Overall, our results show promise for the translation of an FDA-approved anti-osteoporosis drug into a disease-modifying drug for nonspecific LBP, particularly with corroboration of PTH effect on EP sclerosis and aberrant innervation in a large animal model, aged rhesus macaques. We have previously used rhesus macaques to study IVD degeneration by using pingyangmycin, an anti-endothelial drug, sub-EP injection to block the blood vessels in EP (*60*) and an ovariectomized rhesus macaque model to investigate the relationship between IVD degeneration and osteoporosis (*61*). The aged rhesus macaque spontaneously develops IVD degeneration. The current manuscript reports that aberrant innervation of vertebral EPs associated with spinal sensitivity in mice and rhesus macaques is reduced with PTH treatment. Histologically, similar results in EP porosity and sensory innervation in mice and macaques were noted, demonstrating a similar mechanism of PTH action on EP sclerosis between species. Meta-analyses show that a subset of people have improvement in back pain when treated with PTH (*47*). We therefore have proceeded with a randomized double-blind placebo-clinical multicenter trial (registration no. ChiCTR1800018620, SYSU Ethic Committee approved no.2018-053) in patients aged 45 to 65 years with osteopenia, IVD degeneration, and LBP to further investigate the efficacy and duration of PTH(1-34) for the relief of chronic LBP.

## MATERIALS AND METHODS

### Study design

The overall objective of the study was to evaluate whether PTH could attenuate LBP by remodeling sclerotic EP that contributes to sensory innervation and high concentrations of inflammatory factors. We evaluated the spine phenotype in two mouse models: a model of spinal degeneration secondary to mechanical injury in young adult mice and a model of aging-related spinal degeneration. For the mouse studies, each sample size calculation was done in two stages. First, an overall one-way analysis of variance (ANOVA) model was used assuming power of 0.90 and type I error of 0.0125. Second, in the event of a significant main effect, post hoc group testing was performed using Student′s *t* test assuming power of 0.90 and type I error of 0.025. Of the experimental methods in the mouse models, porosity and pressure tolerance testing had the greatest variability. On the basis of our prior studies, assuming observed mean differences between groups and inflating observed variance by 50%, it was estimated that we would need four animals per group at least, whereas post hoc testing required either seven or eight animals per group. All behavioral tests were performed by the same investigator, who was blinded to the study groups. All mouse experimental protocols were approved by the Animal Care and Use Committee of Johns Hopkins University, Baltimore, MD.

Aged rhesus macaques were used as a primate model to more closely mimic humans. All animals used for experiments had IVD degeneration. We did not use any statistical methods to predetermine sample sizes for the rhesus macaque studies. Eight rhesus macaques that met the inclusion criteria were randomly divided into PTH group and vehicle group. All measurements were performed blinded. The study protocol was reviewed and approved by the Institutional Review Board and Ethics Committee of Guangdong Landau Biotechnology Company and the First Affiliated Hospital of Sun Yat-sen University in Guangzhou, China (no. 2018-053).

### Mice

We purchased 104 C57BL/6J (wild-type male mice from Charles River Laboratories, Wilmington, MA). Mice carrying the *Pth1r* gene flanked by loxP sites in the introns flanking the essential E1 exon (*Pth1r* flox/flox) were obtained from the laboratory of H. Kronenberg (*62*). *Noto*Cre mice exhibiting an internal ribosome entry site-nuclear localization signal-Cre recombinase (IRES-NLS-CRE) cassette that replaced exon 2 of the *Noto* locus (*63*) were obtained from C. A. Seguin (*64*). *Pth1r* flox/flox mice and *Noto*Cre mice were crossed to generate mice bearing the *Noto*Cre and a floxed *Pth1r* allele in their germ line as previously reported (*34*). Mice with *Pth1r* conditional deletion in *Noto* lineage cells are referred to as "$Pth1r^{-/-}$" in the text. The genotype of transgenic mice was determined by polymerase chain reaction (PCR) analyses of genomic DNA isolated from mouse tails. The floxed *Pth1r* allele was identified with primers spanning the 3′ loxP site P1 (5′-TGGACGCAGACGATGTCTTTACCA-3′) and P2 (5′-ACATGGCCATGCCTGGGTCTGAGA-3′) according to the prior publication from the laboratory of H. Kronenberg (*62*). The genotyping for the Cre transgene was performed by PCR with the primers Cre F (5′-CAAATAGCCCTGGCAGAT-3′) and Cre R (5′-TGATACAAGGGACATCTTCC-3′). For the aging-induced IVD degeneration model, 72-week-old mice were randomly assigned to either PTH (1-34) (40 μg/kg) or vehicle (phosphate-buffered saline) injected subcutaneously daily for 8 weeks. For the LSI model, after an appropriate level of sedation with ketamine (Vetalar, Ketaset, and Ketalar; 100 mg/kg, intraperitoneally) and xylazine (Rompun, Sedazine, and AnaSed; 10 mg/kg, intraperitoneally), 2-month-old mice underwent resection of the L3 to L5 spinous processes along with the supraspinous and interspinous ligaments to induce instability of

the lumbar spine as previously described (*11*, *19*). Sham operations were performed on a separate group of mice by only detaching the posterior paravertebral muscles from L3 to L5. Eight weeks after LSI or sham surgery, mice were subcutaneously injected with PTH (1-34) (40 μg/kg) or vehicle (phosphate-buffered saline with equivalent volume of PTH) daily. All mice were euthanized 8 weeks after treatment with PTH (1-34) or vehicle ($n$ = 3 to 10 per group; Fig. 1, A and B). All animals were maintained in a 22°C temperature-controlled room with a 12-hour light/12-hour dark cycle at the animal facility of the Johns Hopkins University School of Medicine.

### Rhesus macaques

We purchased 14- to 17-year-old rhesus macaques from Guangdong Landau Biotechnology Company (Guangzhou, China). The age of macaques was chosen on the basis of the macaque age–to–equivalent human age ratio of 1:3.5 (*65*), suggesting that 14- to 17-year-old rhesus macaques represent humans aged about 50 to 60 years. A total of 22 aged male and female macaques were screened by MRI before intervention. A Pfirrmann grade of either 2 or 3 to indicate moderate degree of IVD degeneration was required in the lower lumbar spine (L4-L5, L5-L6, and L6-L7 IVDs) for inclusion in the experimental protocol. Eight macaques were randomly divided into two groups and received either once-daily subcutaneous injection of PTH (1-34) (10 μg/kg) or vehicle (phosphate-buffered saline) for 3 months. All rhesus macaques were euthanized for histological analysis after MRI scanning. The macaques were housed with one animal per cage in a constant 22°C temperature-controlled room with a 12-hour light/12-hour dark cycle.

### MRI acquisition and Pfirrmann grading

MRIs were acquired before intervention and 3 months after intervention with a 1.5-T MR scanner (Achieva, Philips, Amsterdam, Netherlands) with the rhesus macaques lying supine after anesthesia. The imaging protocol included multiple sections of two-dimensional sagittal and axial T1- and T2-weighted fast spin-echo sequences and quantitative MRI acquired with T1ρ and T2 map quantification sequences (table S4) previously developed in our laboratory (*66*) of the lumbar spine (L1-S1). T1ρ values were calculated using Siswin software (version 0.9; Siswin, MR Research Centre at Aarhus University Hospital, Denmark). T2 map values were calculated using Philips DICOM viewer (R3.0-SP12, Philips Healthcare, Amsterdam, Netherlands). The regions of interest were chosen in the center of the nucleus pulposus (0.1 $cm^2$ on images of macaques). Three radiologists who were blinded to the study groups graded all IVDs on the T2-weighted images according to the classification scale of Pfirrmann described as the representative images (fig. S3A) and previously reported (*43*, *66*) as follows: grade I (normal shape, no horizontal bands, and clear distinction of annulus fibrosus and nucleus pulposus), grade II (nonhomogeneous shape with horizontal bands and some blurring between nucleus pulposus and annulus fibrosus), grade III (nonhomogeneous shape with blurring between nucleus pulposus and annulus fibrosus, with annulus fibrosus shape still recognizable), grade IV (nonhomogeneous shape with hypointensity, annulus fibrosus shape not intact, no distinction between nucleus pulposus and annulus fibrosus, and, usually, decreased disc height), and grade V (same as grade IV but collapsed disc space).

### μCT and finite element analysis

Mice and macaques were euthanized and perfusion-fixed with 10% buffered formalin for 5 min via the left ventricle after being flushed with phosphate-buffered saline for 5 to 10 min. The lower thoracic spines and whole lumbar spines of mice were dissected, and the specimens were fixed in 10% buffered formalin for 24 hours and then transferred into phosphate-buffered saline and examined by high-resolution μCT (Skyscan1172, Bruker, Kontich, Belgium). The ribs attached to the lower thoracic spine were included for identification of L3-L5 IVD localization. Images were reconstructed using NRecon, v1.7, software (Bruker) and analyzed using CTAn, v1.16, software (Bruker). We analyzed parameters using three-dimensional model visualization software (CTVol v2.3, Bruker). The scanner was set to a voltage of 55 kVp, a current of 181 μA, and a resolution of 9.0 μm per pixel (for mice) or 16.0 μm per pixel (for macaques) to measure the EP. Coronal images of the L3-L4 and L4-L5 IVDs (mice) or L4-L5, L5-L6, and L6-L7 IVDs (rhesus macaques) were used to perform three-dimensional histomorphometric analyses of EPs. EP volume was defined as the visible EP adjacent to the vertebrae. Three-dimensional structural parameters analyzed were total porosity, total tissue volume (TV), and volume of porosity (Po.V). Finite element analysis in the EP was performed with Mimics (Materialise, Belgium) and Abaqus (Dassault, France) software on the basis of μCT data. The following were used: elastic modulus, $E$ = 0.1 GPa; Poisson′s ratio, μ = 0.28; bone density, ρ = 1700 kg/$cm^3$; and pressure on the EP, 1.2 MPa. $U$ magnitude and von Mises stress were calculated.

### Blood tests

Blood samples of each rhesus macaque were collected after MRI under anesthesia by a trained phlebotomist for measurement of the following: serum calcium (Ca), phosphorus (Ph), procollagen I intact N-terminal, C-terminal cross-linking telopeptide of type I collagen (beta-CrossLaps, Beta-CTx), serum osteocalcin, and alkaline phosphatase, which were conducted by Guangzhou KingMed Diagnostics Group Co. Ltd.

### Enzyme-linked immunosorbent assay

The concentration of EP $PGE_2$ was determined by crushing and lysing pooled L3-L5 vertebral EPs (three mice per group) and using the ELISA Development Kit (KGE004B, R&D Systems Inc., Minneapolis, MN) according to the manufacturer′s instructions. Experimental results were repeated in triplicate.

### Calcein-Alizarin double staining

Mice were intraperitoneally injected with fluorochrome-labeled calcein green (10 mg/kg, Sigma-Aldrich, St. Louis, MO) 9 days before end point. Seven days later, the mice were injected with Alizarin Red (50 mg/kg, Sigma-Aldrich). On the day of end point (2 days after the second injection), we fixed the spine specimens in 70% ethanol for hard tissue slices and Masson-Goldner trichrome staining using standard protocols. The calcein- and Alizarin-labeled EP cavities were observed and captured using a BX51 microscope (Olympus, Tokyo, Japan).

### Retrograde tracing

Six mice per group of Sham, LSI+Veh, LSI+PTH, Aging+Veh, and Aging+PTH (Fig. 1, A and B) were used to perform the retrograde nerve tracing experiment as described previously (*19*). Briefly, we

anesthetized the mice with ketamine and xylazine at 8 weeks after PTH or vehicle treatment. The caudal EP of L4-L5 was exposed with a ventral approach, and 2 μl of Dil (2 mg/ml in methanol; Molecular Probes) was injected into the left part of caudal EP of L4-L5 using borosilicate glass capillaries after drilling a hole at the left part of the EP. The drilling holes were then sealed with bone wax to prevent tracer leakage. The muscle and skin were sutured, and a heating pad was used to protect mice during recovery from anesthesia. Mice were euthanized with an overdose of isoflurane inhalation, and DRGs (L1, L2) were isolated at 1 week after Dil injection. To further classify nerve fiber type (*67*), 10-μm-thick frozen sections were used for coimmunofluorescence staining with PGP9.5 (1:100; ab10404, Abcam), CGRP (1:100; ab81887, Abcam), PIEZO2 (1:300; ab243416, Abcam), NF200 (1:500; ab5539, Millipore), IB4 (1:100; I21411, Thermo Fisher Scientific), and P2X3 (1:500; ab10269, Abcam), and the Dil signals were inspected under 564-nm excitation using a confocal microscope (LSM780, Zeiss). Dil + cells were counted only when the Dil signal was located within the cytoplasm of the cells.

### Histochemistry, immunohistochemistry, and histomorphometry

At the time of euthanasia, the L3-L5 lumbar spines in mice and the L4-L7 IVDs in rhesus macaques were collected and fixed in 10% buffered formalin for 48 hours or overnight. Spine samples were completely decalcified (about 5 days) in 0.5 M EDTA (pH 7.4) and embedded in paraffin or optimal cutting temperature compound (Sakura Finetek, Torrance, CA). Using a standard protocol, we processed 4-μm-thick coronal sections of the L4-L5 lumbar spine for Safranin O and Fast Green, tartrate-resistant acid phosphatase (Sigma-Aldrich), and immunohistochemical staining. We prepared 30-μm-thick coronal sections for sensory nerve– and blood vessel–related immunofluorescence staining, whereas 10-μm-thick coronal sections were used for other immunofluorescence staining using a standard protocol. The sections were incubated overnight at 4°C with primary antibodies to mouse endomucin (1:50; sc-65495, Santa Cruz Biotechnology Inc., Dallas, TX), CD31 conjugated to Alexa Fluor 488 (1:100; FAB3628G, R&D Systems), PGP9.5 (1:100; ab10404, Abcam, Cambridge, UK), and COX-2 (1:100; ab15191, Abcam). Then, the corresponding secondary antibodies were added onto the sections for 1 hour while avoiding light. For immunohistochemistry, a horseradish peroxidase–streptavidin detection system (Dako, Agilent, Santa Clara, CA) was used to detect immunoactivity, followed by counterstaining with hematoxylin (Sigma-Aldrich). For immunofluorescence staining, the sections were counterstained with 4′,6-diamidino-2-phenylindole (H-1200 DAPI, Vector Laboratories, Burlingame, CA). The sample images were observed and captured using a BX51 or DP71 microscope (Olympus, Tokyo, Japan) or LSM780 confocal microscope (Zeiss, Oberkochen, Germany). ImageJ software (National Institutes of Health, Bethesda, MD) was used for quantitative analysis.

### mRNA sequence screen

Ten LSI-model mice were divided into two groups treated with either vehicle ($n$ = 4) or PTH ($n$ = 6) for 8 weeks. L3-L4, L4-L5, and L5-S1 EP tissue were used to obtain an mRNA sequence screen (Kangchen Biotech, Shanghai, China), and the raw data of all differentially expressed genes can be found in data file S2.

### Animal behavioral tests

#### *Pressure hyperalgesia*

The vocalization threshold, based on the force of an applied force gauge (SMALGO, Bioseb, Pinellas Park, FL), was measured by pressing a 5-mm-diameter device tip directly on the dorsal skin over L4-L5 while the mice were gently restrained. The force was increased at about 50*g*/s until an audible vocalization was heard. A cutoff force of 400*g* was used to prevent tissue trauma. Two tests were performed at 15-min intervals, and the mean value was used as the nociceptive threshold.

#### *Spontaneous activity (spontaneous wheel running)*

Spontaneous wheel running activity was recorded using activity wheels designed for mice (model BIO-ACTIVW-M, Bioseb). Software enabled recording of activity within a cage similar to the mice′s home cage with dimensions of 35 cm by 20 cm by 13 cm. The wheel (diameter, 23 cm; lane width, 5 cm) could be turned in both directions and was connected to an analyzer that automatically recorded running activity. The animals had food and water available ad libitum. We evaluated the distance traveled (expressed in meters), maximum speed, and total active time during the 2 days of evaluation for each animal.

### Statistics

All data analyses were performed using SPSS, version 22.0, software (IBM Corp., Armonk, NY). Data are presented as means ± SD. We used unpaired, two-tailed Student′s $t$ tests for mouse data comparisons between two groups or paired Student′s $t$ tests between different time points within one group for mouse data that followed a normal distribution. For data that did not follow a normal distribution, Mann-Whitney test was used. For comparisons among multiple groups, we used one-way ANOVA with Bonferroni′s post hoc test. Because of the hierarchical nature of MRI rhesus macaque data, we used multilevel random effects regression models, which allowed between-macaque differences in mean levels (intercepts) and within-relations (slopes) to vary randomly. The open-source R software version 3.6.2 (lme4, lmerTest, ordinal, and tableone packages) was used for statistical analysis. After assumptions of regression models (normality of distribution, linearity, and error homogeneity) were evaluated and confirmed, we compared longitudinal MRI measurements (dependent variables, i.e., outcomes) between PTH and vehicle treatment groups using linear (for continuous outcome variables: T1ρ and T2 map) and logistic (for categorical outcome variable: Pfirrmann grade) mixed-effect regression models. The interaction of time and treatment group was defined as the independent variable of interest. For all experiments, $P < 0.05$ was considered significant. All inclusion/exclusion criteria were preestablished, and no samples or animals were excluded from analysis. The experiments were randomized, and the investigators were blinded to allocation during experiments and outcome assessments.

## Supplementary Materials

**This PDF file includes:**
Figs. S1 to S5
Tables S1 to S4

**Other Supplementary Material for this manuscript includes the following:**
Data files S1 to S3
MDAR Reproducibility Checklist

## REFERENCES AND NOTES


1. B. I. Martin, R. A. Deyo, S. K. Mirza, J. A. Turner, B. A. Comstock, W. Hollingworth, S. D. Sullivan, Expenditures and health status among adults with back and neck problems. *JAMA* **299**, 656–664 (2008).
2. S. Clark, R. Horton, Low back pain: A major global challenge. *Lancet* **391**, 2302 (2018).
3. D. I. Rubin, Epidemiology and risk factors for spine pain. *Neurol. Clin.* **25**, 353–371 (2007).
4. F. Taher, D. Essig, D. R. Lebl, A. P. Hughes, A. A. Sama, F. P. Cammisa, F. P. Girardi, Lumbar degenerative disc disease: Current and future concepts of diagnosis and management. *Adv. Orthop.* **2012**, 970752 (2012).
5. D. Samartzis, T. B. Grivas, Thematic series—Low back pain. *Scoliosis Spinal Disord.* **12**, 1 (2017).
6. C. Maher, M. Underwood, R. Buchbinder, Non-specific low back pain. *LANCET* **389**, 736–747 (2017).
7. R. W. McGorry, B. S. Webster, S. H. Snook, S. M. Hsiang, The relation between pain intensity, disability, and the episodic nature of chronic and recurrent low back pain. *Spine* **25**, 834–841 (2000).
8. A. J. Fields, A. Ballatori, E. C. Liebenberg, J. C. Lotz, Contribution of the endplates to disc degeneration. *Curr. Mol. Biol. Rep.* **4**, 151–160 (2018).
9. Y. Wang, T. Videman, M. C. Battie, ISSLS prize winner: Lumbar vertebral endplate lesions: Associations with disc degeneration and back pain history. *Spine* **37**, 1490–1496 (2012).
10. J. C. Lotz, A. J. Fields, E. C. Liebenberg, The role of the vertebral end plate in low back pain. *Global Spine J.* **3**, 153–164 (2013).
11. G. Paesold, A. G. Nerlich, N. Boos, Biological treatment strategies for disc degeneration: Potentials and shortcomings. *Eur. Spine J.* **16**, 447–468 (2007).
12. T. Grunhagen, A. Shirazi-Adl, J. C. T. Fairbank, J. P. Urban, Intervertebral disk nutrition: A review of factors influencing concentrations of nutrients and metabolites. *Orthop. Clin. North Am.* **42**, 465–477 (2011).
13. Q. Bian, L. Ma, A. Jain, J. L. Crane, K. Kebaish, M. Wan, Z. Zhang, G. X. Edward, P. D. Sponseller, C. A. Seguin, L. H. Riley, Y. Wang, X. Cao, Mechanosignaling activation of TGFβ maintains intervertebral disc homeostasis. *Bone Res.* **5**, 17008 (2017).
14. Q. Bian, A. Jain, X. Xu, K. Kebaish, J. L. Crane, Z. Zhang, M. Wan, L. Ma, L. H. Riley, P. D. Sponseller, X. E. Guo, W. W. Lu, Y. Wang, X. Cao, Excessive activation of TGFβ by spinal instability causes vertebral endplate sclerosis. *Sci. Rep.* **6**, 27093 (2016).
15. A. G. Rodriguez, A. E. Rodriguez-Soto, A. J. Burghardt, S. Berven, S. Majumdar, J. C. Lotz, Morphology of the human vertebral endplate. *J. Orthop. Res.* **30**, 280–287 (2012).
16. A. J. Fields, E. C. Liebenberg, J. C. Lotz, Innervation of pathologies in the lumbar vertebral end plate and intervertebral disc. *Spine J.* **14**, 513–521 (2014).
17. T. S. Jensen, J. Karppinen, J. S. Sorensen, J. Niinimaki, C. Leboeuf-Yde, Vertebral endplate signal changes (Modic change): A systematic literature review of prevalence and association with non-specific low back pain. *Eur. Spine J.* **17**, 1407–1422 (2008).
18. R. Rahme, R. Moussa, The modic vertebral endplate and marrow changes: Pathologic significance and relation to low back pain and segmental instability of the lumbar spine. *AJNR Am. J. Neuroradiol.* **29**, 838–842 (2008).
19. S. Ni, Z. Ling, X. Wang, Y. Cao, T. Wu, R. Deng, J. L. Crane, R. Skolasky, S. Demehri, G. Zhen, A. Jain, P. Wu, D. Pan, B. Hu, X. Lyu, Y. Li, H. Chen, H. Qi, Y. Guan, X. Dong, M. Wan, X. Zou, H. Lu, J. Hu, X. Cao, Sensory innervation in porous endplates by Netrin-1 from osteoclasts mediates PGE2-induced spinal hypersensitivity in mice. *Nat. Commun.* **10**, 5643 (2019).
20. K. Luoma, T. Vehmas, L. Kerttula, M. Gronblad, E. Rinne, Chronic low back pain in relation to Modic changes, bony endplate lesions, and disc degeneration in a prospective MRI study. *Eur. Spine J.* **25**, 2873–2881 (2016).
21. J. Jarvinen, J. Karppinen, J. Niinimaki, M. Haapea, M. Gronblad, K. Luoma, E. Rinne, Association between changes in lumbar Modic changes and low back symptoms over a two-year period. *BMC Musculoskelet. Disord.* **16**, 98 (2015).
22. J. Saukkonen, J. Maatta, P. Oura, E. Kyllonen, O. Tervonen, J. Niinimaki, J. Auvinen, J. Karppinen, Association between Modic changes and low back pain in middle age: A Northern Finland Birth Cohort study. *Spine* **45**, 1360–1367 (2020).
23. S. Ohtori, G. Inoue, T. Ito, T. Koshi, T. Ozawa, H. Doya, T. Saito, H. Moriya, K. Takahashi, Tumor necrosis factor-immunoreactive cells and PGP 9.5-immunoreactive nerve fibers in vertebral endplates of patients with discogenic low back Pain and Modic Type 1 or Type 2 changes on MRI. *Spine* **31**, 1026–1031 (2006).
24. Z. Ling, L. Li, Y. Chen, H. Hu, X. Zhao, J. Wilson, Q. Qi, D. Liu, F. Wei, X. Chen, J. Lu, Z. Zhou, X. Zou, Changes of the end plate cartilage are associated with intervertebral disc degeneration: A quantitative magnetic resonance imaging study in rhesus monkeys and humans. *J. Orthop. Translat.* **24**, 23–31 (2020).
25. H. E. Gruber, B. Gordon, C. Williams, H. J. Norton, E. J. Hanley Jr., Vertebral endplate and disc changes in the aging sand rat lumbar spine: Cross-sectional analyses of a large male and female population. *Spine* **32**, 2529–2536 (2007).
26. S. Bernick, R. Cailliet, Vertebral end-plate changes with aging of human vertebrae. *Spine* **7**, 97–102 (1982).
27. J. L. Crane, X. Cao, Bone marrow mesenchymal stem cells and TGF-β signaling in bone remodeling. *J. Clin. Invest.* **124**, 466–472 (2014).
28. J. Pfeilschifter, F. Laukhuf, B. Muller-Beckmann, W. F. Blum, T. Pfister, R. Ziegler, Parathyroid hormone increases the concentration of insulin-like growth factor-I and transforming growth factor beta 1 in rat bone. *J. Clin. Invest.* **96**, 767–774 (1995).
29. M. Wan, C. Yang, J. Li, X. Wu, H. Yuan, H. Ma, X. He, S. Nie, C. Chang, X. Cao, Parathyroid hormone signaling through low-density lipoprotein-related protein 6. *Genes Dev.* **22**, 2968–2979 (2008).
30. P. Watson, D. Lazowski, V. Han, L. Fraher, B. Steer, A. Hodsman, Parathyroid hormone restores bone mass and enhances osteoblast insulin-like growth factor I gene expression in ovariectomized rats. *Bone* **16**, 357–365 (1995).
31. R. L. Jilka, M. Almeida, E. Ambrogini, L. Han, P. K. Roberson, R. S. Weinstein, S. C. Manolagas, Decreased oxidative stress and greater bone anabolism in the aged, when compared to the young, murine skeleton with parathyroid hormone administration. *Aging Cell* **9**, 851–867 (2010).
32. E. Canalis, M. Centrella, W. Burch, T. L. McCarthy, Insulin-like growth factor I mediates selective anabolic effects of parathyroid hormone in bone cultures. *J. Clin. Invest.* **83**, 60–65 (1989).
33. T. Qiu, X. Wu, F. Zhang, T. L. Clemens, M. Wan, X. Cao, TGF-beta type II receptor phosphorylates PTH receptor to integrate bone remodelling signalling. *Nat. Cell Biol.* **12**, 224–234 (2010).
34. L. Zheng, Y. Cao, S. Ni, H. Qi, Z. Ling, X. Xu, X. Zou, T. Wu, R. Deng, B. Hu, B. Gao, H. Chen, Y. Li, J. Zhu, F. Tintani, S. Demehri, A. Jain, K. M. Kebaish, S. Liao, C. A. Seguin, J. L. Crane, M. Wan, H. Lu, P. D. Sponseller, L. R. Riley, X. Zhou, J. Hu, X. Cao, Ciliary parathyroid hormone signaling activates transforming growth factor-β to maintain intervertebral disc homeostasis during aging. *Bone Res.* **6**, 21 (2018).
35. Q. Sun, G. Zhen, T. P. Li, Q. Guo, Y. Li, W. Su, P. Xue, X. Wang, M. Wan, Y. Guan, X. Dong, S. Li, M. Cai, X. Cao, Parathyroid hormone attenuates osteoarthritis pain by remodeling subchondral bone in mice. *eLife* **10**, e66532 (2021).
36. F. D. Zhao, P. Pollintine, B. D. Hole, M. A. Adams, P. Dolan, Vertebral fractures usually affect the cranial endplate because it is thinner and supported by less-dense trabecular bone. *Bone* **44**, 372–379 (2009).
37. P. A. Hulme, S. K. Boyd, S. J. Ferguson, Regional variation in vertebral bone morphology and its contribution to vertebral fracture strength. *Bone* **41**, 946–957 (2007).
38. N. A. Langrana, S. P. Kale, W. T. Edwards, C. K. Lee, K. J. Kopacz, Measurement and analyses of the effects of adjacent end plate curvatures on vertebral stresses. *Spine J.* **6**, 267–278 (2006).
39. S. Dudli, W. Enns-Bray, Y. Pauchard, A. Rommeler, A. J. Fields, S. J. Ferguson, B. Helgason, Larger vertebral endplate concavities cause higher failure load and work at failure under high-rate impact loading of rabbit spinal explants. *J. Mech. Behav. Biomed. Mater.* **80**, 104–110 (2018).
40. A. P. Kusumbe, S. K. Ramasamy, R. H. Adams, Coupling of angiogenesis and osteogenesis by a specific vessel subtype in bone. *Nature* **507**, 323–328 (2014).
41. H. Xie, Z. Cui, L. Wang, Z. Xia, Y. Hu, L. Xian, C. Li, L. Xie, J. Crane, M. Wan, G. Zhen, Q. Bian, B. Yu, W. Chang, T. Qiu, M. Pickarski, L. T. Duong, J. J. Windle, X. Luo, E. Liao, X. Cao, PDGF-BB secreted by preosteoclasts induces angiogenesis during coupling with osteogenesis. *Nat. Med.* **20**, 1270–1278 (2014).
42. S. Ohtori, G. Inoue, M. Miyagi, K. Takahashi, Pathomechanisms of discogenic low back pain in humans and animal models. *Spine J.* **15**, 1347–1355 (2015).
43. C. W. Pfirrmann, A. Metzdorf, M. Zanetti, J. Hodler, N. Boos, Magnetic resonance classification of lumbar intervertebral disc degeneration. *Spine* **26**, 1873–1878 (2001).
44. R. Chou, L. H. Huffman; American Pain Society; American College of Physicians, Medications for acute and chronic low back pain: A review of the evidence for an American Pain Society/American College of Physicians clinical practice guideline. *Ann. Intern. Med.* **147**, 505–514 (2007).
45. P. P. Raj, Intervertebral disc: Anatomy-physiology-pathophysiology-treatment. *Pain Pract.* **8**, 18–44 (2008).
46. D. A. Levin, J. A. Bendo, M. Quirno, T. Errico, J. Goldstein, J. Spivak, Comparative charge analysis of one- and two-level lumbar total disc arthroplasty versus circumferential lumbar fusion. *Spine* **32**, 2905–2909 (2007).
47. M. C. Nevitt, P. Chen, R. K. Dore, J. Y. Reginster, D. P. Kiel, J. R. Zanchetta, E. V. Glass, J. H. Krege, Reduced risk of back pain following teriparatide treatment: A meta-analysis. *Osteoporos. Int.* **17**, 273–280 (2006).
48. K. Eastman, M. Gerlach, I. Piec, J. Greeves, W. Fraser, Effectiveness of parathyroid hormone (PTH) analogues on fracture healing: A meta-analysis. *Osteoporos. Int.* **32**, 1531–1546 (2021).
49. K. Luoma, H. Riihimaki, R. Luukkonen, R. Raininko, E. Viikari-Juntura, A. Lamminen, Low back pain in relation to lumbar disc degeneration. *Spine* **25**, 487–492 (2000).

50. N. Boos, S. Weissbach, H. Rohrbach, C. Weiler, K. F. Spratt, A. G. Nerlich, Classification of age-related changes in lumbar intervertebral discs: 2002 Volvo Award in basic science. *Spine* **27**, 2631–2644 (2002).
51. J. M. Lee, J. Y. Song, M. Baek, H. Y. Jung, H. Kang, I. B. Han, Y. D. Kwon, D. E. Shin, Interleukin-1β induces angiogenesis and innervation in human intervertebral disc degeneration. *J. Orthop. Res.* **29**, 265–269 (2011).
52. A. L. Binch, A. A. Cole, L. M. Breakwell, A. L. Michael, N. Chiverton, A. K. Cross, C. L. Le Maitre, Expression and regulation of neurotrophic and angiogenic factors during human intervertebral disc degeneration. *Arthritis Res. Ther.* **16**, 416 (2014).
53. J. Aoki, I. Yamamoto, N. Kitamura, T. Sone, H. Itoh, K. Torizuka, K. Takasu, End plate of the discovertebral joint: Degenerative change in the elderly adult. *Radiology* **164**, 411–414 (1987).
54. R. J. Moore, The vertebral end-plate: What do we know? *Eur. Spine J.* **9**, 92–96 (2000).
55. J. Mizrahi, M. J. Silva, T. M. Keaveny, W. T. Edwards, W. C. Hayes, Finite-element stress analysis of the normal and osteoporotic lumbar vertebral body. *Spine* **18**, 2088–2096 (1993).
56. E. R. Sampson, M. J. Hilton, Y. Tian, D. Chen, E. M. Schwarz, R. A. Mooney, S. V. Bukata, R. J. O'Keefe, H. Awad, J. E. Puzas, R. N. Rosier, M. J. Zuscik, Teriparatide as a chondroregenerative therapy for injury-induced osteoarthritis. *Sci. Transl. Med.* **3**, 101ra93 (2011).
57. H. Chen, B. Hu, X. Lv, S. Zhu, G. Zhen, M. Wan, A. Jain, B. Gao, Y. Chai, M. Yang, X. Wang, R. Deng, L. Wang, Y. Cao, S. Ni, S. Liu, W. Yuan, H. Chen, X. Dong, Y. Guan, H. Yang, X. Cao, Prostaglandin E2 mediates sensory nerve regulation of bone homeostasis. *Nat. Commun.* **10**, 181 (2019).
58. A. D. Bakker, M. Joldersma, J. Klein-Nulend, E. H. Burger, Interactive effects of PTH and mechanical stress on nitric oxide and PGE2 production by primary mouse osteoblastic cells. *Am. J. Physiol. Endocrinol. Metab.* **285**, E608–E613 (2003).
59. M. Coetzee, M. Haag, N. Claassen, M. C. Kruger, Stimulation of prostaglandin E2 (PGE2) production by arachidonic acid, oestrogen and parathyroid hormone in MG-63 and MC3T3-E1 osteoblast-like cells. *Prostaglandins Leukot. Essent. Fatty Acids* **73**, 423–430 (2005).
60. F. Wei, R. Zhong, L. Wang, Z. Zhou, X. Pan, S. Cui, H. Sun, X. Zou, M. Gao, B. Jiang, W. Chen, W. Zhuang, H. Sun, S. Liu, Pingyangmycin-induced in vivo lumbar disc degeneration model of rhesus monkeys. *Spine* **40**, E199–E210 (2015).
61. R. Zhong, F. Wei, L. Wang, S. Cui, N. Chen, S. Liu, X. Zou, The effects of intervertebral disc degeneration combined with osteoporosis on vascularization and microarchitecture of the endplate in rhesus monkeys. *Eur. Spine J.* **25**, 2705–2715 (2016).
62. T. Kobayashi, U. I. Chung, E. Schipani, M. Starbuck, G. Karsenty, T. Katagiri, D. L. Goad, B. Lanske, H. M. Kronenberg, PTHrP and Indian hedgehog control differentiation of growth plate chondrocytes at multiple steps. *Development* **129**, 2977–2986 (2002).
63. M. R. McCann, O. J. Tamplin, J. Rossant, C. A. Seguin, Tracing notochord-derived cells using a Noto-cre mouse: Implications for intervertebral disc development. *Dis. Model. Mech.* **5**, 73–82 (2012).
64. J. Bedore, W. Sha, M. R. McCann, S. Liu, A. Leask, C. A. Seguin, Impaired intervertebral disc development and premature disc degeneration in mice with notochord-specific deletion of CCN2. *Arthritis Rheum.* **65**, 2634–2644 (2013).
65. A. E. Duncan, R. J. Colman, P. A. Kramer, Sex differences in spinal osteoarthritis in humans and rhesus monkeys (*Macaca mulatta*). *Spine* **37**, 915–922 (2012).
66. Z. Zhou, B. Jiang, Z. Zhou, X. Pan, H. Sun, B. Huang, T. Liang, S. Ringgaard, X. Zou, Intervertebral disk degeneration: T1ρ MR imaging of human and animal models. *Radiology* **268**, 492–500 (2013).
67. D. Usoskin, A. Furlan, S. Islam, H. Abdo, P. Lonnerberg, D. Lou, J. Hjerling-Leffler, J. Haeggstrom, O. Kharchenko, P. V. Kharchenko, S. Linnarsson, P. Ernfors, Unbiased classification of sensory neuron types by large-scale single-cell RNA sequencing. *Nat. Neurosci.* **18**, 145–153 (2015).


**Acknowledgments:** We thank the editorial services group of the Department of Orthopaedic Surgery for editing this manuscript. **Funding:** This work is supported by FOX Gift and Necrosis Fund from the Johns Hopkins Department of Orthopaedic Surgery (X.C.). **Author contributions:** Z.L. and J.C. conceived the experimental designs, conducted most of the experiments, and prepared the manuscript. H.H., Y.C., and X.Z. helped with the rhesus macaques' radiology examinations. Y.C. and S.N. helped with animal surgery and histology sections. H.H., S.D., and B.M. helped with data collection and analysis. J.C., M.W., and X.P. provided ideas for the experiments and the project. X.C. and X.Z. conceived the idea, supervised the project, outlined and revised the manuscript. **Competing interests:** Patents in protection of PTH effects on spine degeneration and pain have been filed by John Hopkins University (PCT/US2018/016429 "Parathyroid hormone stimulates regeneration of degenerative discs disease"; PCT/US2020/062879 "Parathyroid hormone attenuates low back pain and osteoarthritis pain" and U.S. Application No. 17/191,419 "Parathyroid hormone and regeneration of degenerative discs disease"). The authors declare no other competing interests. **Data and materials availability:** All data are available in the main text or the Supplementary Materials. All materials used in the study are commercially available. Floxed *Pth1r* (*Pth1r*flox/flox) mice were obtained from the laboratory of H. Kronenberg at Harvard University and the *Noto*-Cre mice from C. A. Seguin at University of Western Ontario through material transfer agreements.

Submitted 1 February 2023
Accepted 23 October 2023
Published 15 November 2023
10.1126/scitranslmed.adg8982